Towards an IoT Based Water Management System for a Campus

Prachet Verma[1], Akshay Kumar[1], Nihesh Rathod[2], Pratik Jain[1], Mallikarjun S.[1], Renu Subramanian[2], Bharadwaj Amrutur[2,4], M. S. Mohan Kumar[3,4], Rajesh Sundaresan[2]
[1]Department of Electronic Systems Engineering
[2]Electrical Communication Engineering Department
[3]Department of Civil Engineering
[4]Robert Bosch Center for Cyber-Physical Systems,
Indian Institute of Science, Bangalore

***Abstract*— We discuss the design and preliminary results of an IoT based system for management of the water distribution system in a large campus. In particular, we focus on two specific components of the system: a low cost ultrasonic based water level sensor and a sub-GHz based campus scale wireless network to connect the sensors. We describe techniques to achieve a large sensing distance that makes them suitable for installation across overhead tanks (OHT) and ground level reservoirs (GLR). The wireless network, which uses sub-GHz radios, connects to a gateway that can upload the data online for visualisation and analytics.**

***Index Terms*—IoT, Smart cities, Water management, Ultrasonic level measurement**

I. Introduction

Around 1.2 billion people, or almost one-fifth of the world's population, live in areas of water scarcity [1], and by 2025 water scarcity is expected to affect more than 1.8 billion people—hurting agricultural workers and poor farmers the most [2]. Water scarcity is among the main problems to be faced by many societies and the world in the 21st century. Water use has been growing at more than twice the rate of population increase in the last century, and, although there is no global water scarcity as such, an increasing number of regions are chronically short of water [3]. In such places, large storage tanks are used as intermediary buffers to smooth out the water distribution and meet peak demands. In addition, most households and offices also have large local storage tanks to help further mitigate the variability due to the lack of 24x7 water supply from the utilities. Unregulated storage of water can lead to "water hoarding", with storage of up to 7x the daily usage of water in local household tanks in some cities. This leads to inefficient distribution of water to the consumers, especially in times of scarcity.

With the advent of the Internet of Things, the water distribution system is a natural choice for instrumentation with a network of sensors that can communicate with each other and gather data for analytics, so that more efficient distribution and management of water and its related assets is possible.

We have embarked on a project to create a Smart Water Distribution System, with the IISc campus as a test bed. The campus is rather large, with a size of about 2 km × 1 km. Our aim is to instrument the water tanks across the campus (figure 1) on a single wireless sensor network in the first phase.

Fig. 1. Sensor deployment and the corresponding network topology in the IISc campus. The gateway collects the data from the sensors at the OHTs and GLRs and uploads to the internet. OHT sensors connect directly to the gateway and also act as relays for the GLR sensors.

Our key contribution is a low cost ultrasonic water level sensor that can measure the level of water in tanks up to a depth of 10 m, and consequently the volume, in various overhead tanks and ground level reservoirs across the campus. The motivations behind developing ultrasonic water level sensors are two-fold. Firstly, alternative methods of water level measurement, such as a buoy or pressure sensors [4] at the base of the tank, are intrusive and tedious to install and maintain at a large scale. They also come with the risk of contamination. Secondly, the easily available ultrasonic sensors in the market are either short on maximum distance [5], or are too expensive. Our second contribution is a sub-GHz communication network

978-1-4673-6552-9/15/$31.00 ©2015 IEEE

(868-915MHz) to cover the rather large distances between the tanks. This paper describes the design of both the sensor and the network. We begin with related work in section II, followed by describing the design of the sensor in section III. The network is described in section IV, power management is dealt with in section V and results are discussed in section VI.

II. Related Work

In an earlier effort, Kudva et al. [6] proposed a real-time water balance monitoring system for a campus. That work used an off-the-shelf ultrasonic level sensor, HCSR04 [5], which is mounted at the top of the tank. It sends a train of ultrasound pulses at 40 KHz towards the water surface and measures the time to receive the reflected waves by sensing when the reflected edge crosses a threshold. This approach works well when the received signals are large in amplitude and hence its range was limited to about 4 m, which is insufficient for large distribution tanks that can be as deep as 8 m. For such large depths, a correlation based approach should be used to deal with the severe attenuation of the reflected pulses, as well as with multiple reflections.

In another related work, Pipenet [7] uses a Bluetooth based network of sensors to collect data into a cluster head from various regions of the pipe network. The cluster heads then communicate with a server using GSM. The data is analysed to signal leaks or pipe bursts.

In our campus, the water tanks are distributed randomly and some of them are farther than a kilometre away from each other. Hence solutions like Zigbee, WiFi and Bluetooth do not work well. GSM/GPRS is a possible option. However, the power consumption of these modems is significantly high and this drives up the system cost considerably [11]. Hence, we have explored the use of sub-GHz radios to build a wireless network to transfer the sensory information to a gateway. The gateway then uploads the data to a cloud.

III. Ultrasound Based Water Level Sensor

As mentioned in section I, we needed to develop a low cost water level sensor that can work in tanks having a depth of up to 10 m. We have used an ultrasound based system as this allows us to mount the sensors outside the water. We use a pair of ultrasonic transducers that are mounted under the lid of the tank. The ultrasound pulses reflect off the surface of the water and are picked up by the receiving transducer. The time of flight between transmitted and received ultrasound is measured to obtain the distance between the top of the tank and the surface of water. Given the dimensions of the tank, the volume of water is computed.

One of the key design requirements is to achieve good energy efficiencies so that long battery operation is achieved. Keeping this in mind, the design of the sensor is briefly described next.

A. Transducer Characterisation

The ultrasonic transducers can be modelled by the Extended Butterworth-Van Dyke Model as shown in figure 2. These transducers are found to have multiple resonant frequencies, which is the reason this model was chosen, since each RLC branch represents one resonant frequency. To derive the values of components in the model, the transducer is characterised using an impedance analyser for frequencies between 1 kHz to 100 kHz at 800 points. At frequencies well above the resonant frequencies, R_s, L_s and C_s have negligible influence on the impedance curve, and the impedance equals C_0. At series resonant frequency, L_s and C_s cancel each other out, and the impedance equals the parallel combination of R_s and C_0. We thus obtain the equations for the resonant frequencies as:

Series resonance: $\omega_s = \frac{1}{\sqrt{L_s C_s}}$

Parallel resonance: $\omega_p = \frac{1}{\sqrt{L_s C_{eq}}}$ where $C_{eq} = \frac{C_0 C_s}{C_0 + C_s}$

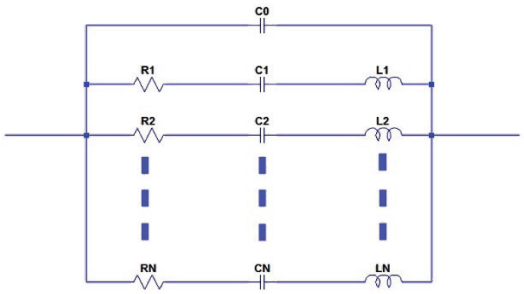

Fig. 2. Extended BVD Model of the ultrasonic transducer

As there are two unknowns and two equations, L and C values can be found easily. For different pairs of resonant frequencies, different R, L and C values are calculated. In our experiments we found two or three resonant peaks depending on the transducer. At a time, only one RLC branch is considered and others are neglected. As highlighted in [8], this method does not work when two resonant peaks are very close to each other, because, in that case, the series resonant frequency of the second peak would be ambiguous. In our low-cost transducers, the two peaks lie around 40 kHz and 52 kHz, respectively.

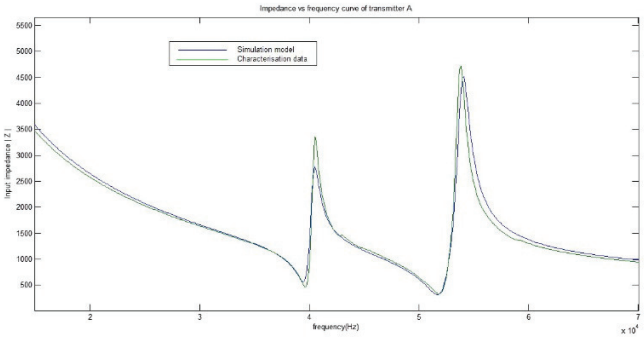

Fig. 3. Comparison of simulated and experimental data of Impedance vs. Frequency curve of transducer.

B. Maximising transmitted energy

To maximise energy efficiency, it is important to transmit at the resonant frequencies. The impedance curve of the piezoelectric transducer shows two peaks and deals with only the electrical properties of the transducer. Some part of electrical energy dissipated across the resistor gets converted to acoustic waves. Though simulations of the derived model suggest that power transmitted at the two resonant frequencies should be similar, it is practically observed that:

$$\frac{P_{TX}@(52kHz)}{P_{TX}@(40kHz)} \neq \frac{P_{RES}@(52kHz)}{P_{RES}@(40kHz)}$$

Here, P_{TX} is the power transmitted into the medium and P_{RES} is the power dissipated across the resistor. This indicates that there is a difference in efficiency of electrical to mechanical energy conversion at different resonant frequencies due to mechanical loading.

To increase the range, higher signal energies need to be transmitted. This can be achieved by increasing the voltage amplitude of excitation of the transmitter. However, increasing the voltage beyond a certain point does not provide a commensurate improvement in the received signal strength. Instead, we increase the number of pulses transmitted so that our correlation based receiver can see a larger signal energy. We also observe that due to inertia, the piezoelectric transducer takes some time to build up to maximum amplitude, which puts a lower bound on the minimum pulse duration for the excitation.

C. Transmitter Circuit

A block diagram of the transmitter circuit is shown below.

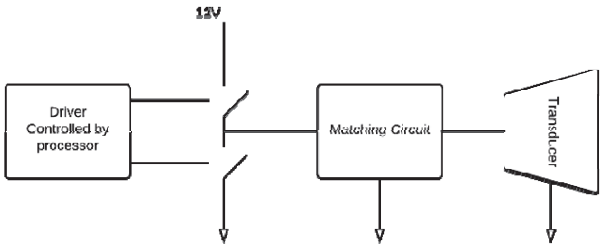

Fig. 4. Block diagram of transmitter

The driver circuit chosen for the transmitter is a push-pull output driver (Totem Pole Output). An LC matching circuit [9] has been used for matching the transducer and switching network. The components values for the matching circuits are derived from the Extended BVD Model for the 40 kHz branch.

D. Receiver Circuit

The block diagram of the receiver is shown below.

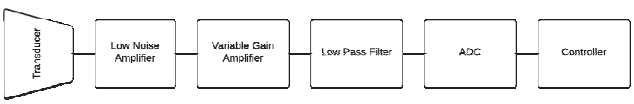

Fig. 5. Block diagram of receiver

The amplifier used is the TI VCA2615, which is a two-stage voltage controlled amplifier (VCA) consisting of a Low–Noise Preamplifier (LNP) and a Voltage Gain Amplifier (VGA). We need controllable gain because the amplifier will saturate under high gain if the reflecting surface is close to the transmitter, and when the reflecting surface is far and the gain is low, the amplifier will not amplify the signal above the noise floor. The differential output of the amplifier is converted to single ended signal and sent to a passive low pass filter (RC), which can also be considered as an AM demodulator for envelope detection. The RC filter also serves as an anti-aliasing filter.

E. Measurement

The microcontroller used is the TI MSP432P401R 32-bit ARM core M4 with 64 kB RAM. The water level is measured once every minute. The gain of the amplifier and the number of cycles transmitted are set based on the previous reading of distance, since the level of water is expected to change gradually. The controller then switches the transmitter's driver circuit such that a Barker code [10] is transmitted by the transducer. Barker codes are finite sequences of lengths between 3 and 13, having very sharp autocorrelation functions with small side lobes. The 5-bit Barker code, {+1, +1, +1, -1, +1} is used for transmission. Once the transmission is complete, the controller's 14-bit ADC starts recording at 200 kSamples/s for 68 ms, recording a total of 13600 samples. This data is saved in the controller's RAM, where an in situ correlation with the transmitted pattern is done to obtain a peak which corresponds to the reflection off the surface of water. The parameters (frequency, sampling rate and duration of sampling) are all configurable.

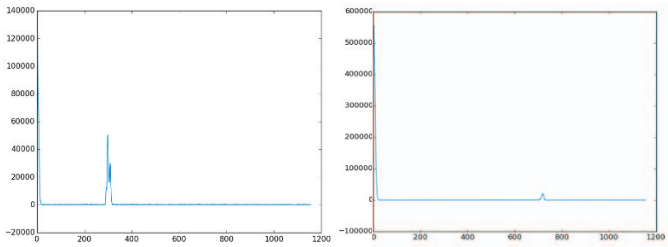

Fig. 6. Correlated data from controller for 3m and 7.2m

Since the gain is set based on the previous reading of distance, an initialisation sequence is needed to set the gain for the first reading. For the first reading, the controller first sets the gain for the midpoint, i.e., 5 m, and then iterates through the range hunting for the actual reading. The initialisation sequence takes between 5 and 11 readings to pin-point the distance. Subsequently, one reading is taken per sample. If the distance measured is not in the vicinity of the previous reading, a second reading is taken. If the reading is still not in the vicinity, the system reinitialises.

IV. Network

A. Network nodes

There are three types of nodes in the network:

1) Gateway

The gateway receives data from all sensors and forwards it to the cloud based server, and receives commands from gateway server and transmits them to the sensors (end nodes). The gateway radio is always in receiver mode. But once a packet is received, it checks for pending commands for the sender and transmits them, if any, and then switches back to receive mode. Every command has to be acknowledged by an ACK bit in the next packet from that sensor node, failing which the command is retransmitted.

2) End nodes

The end nodes are at the edge of the network and are attached to the sensors. To achieve low power, they are duty-cycled to wake up periodically, collect data from connected sensors and transmit them to the gateway. Immediately after a transmission, they enter into the receive mode for a very short duration (200 ms) to receive any commands, before going to sleep. These nodes also support an additional command-enabled low power mode of operation, wherein the frequency of communication is reduced, while frequency of reading from sensors is unchanged. This allows packing a number of sensor readings into a single radio transmission.

3) Relay nodes

These are modified end nodes that can also behave as a relay for some other end node. So they can not only transmit data from their own sensor, but also relay the data from another end node that peers with it. They are configured to retransmit the end node packets they receive. These nodes support two-way communication and can relay commands from the gateway to the end nodes.

B. Network design

Rathod et al. [11] compare two sub-GHz radios, Texas Instruments CC1200-DK and Semtech LoRa iM880A. The IISc campus was categorised into various environment types, and the path loss exponent was estimated in each environment type. The key results of the survey indicated that in clear line-of-sight, the CC1200-DK performs better in Packet Error Rate (PER), whereas with foliage and obstructions, iM880A marginally outperforms CC1200-DK, due to a better physical layer. TI CC1200-DK gives better RSSI and header efficiency, and is therefore the sub-GHz radio selected for the implementation of the network. It can transmit up to 14 dBm, thereby improving its range and reducing its PER. The survey results of [11] indicated that it is possible to have a star network for all the overhead tanks (OHT), but the challenge is to connect the ground level reservoirs (GLR) to the network; as their ground level prevents line of sight communication to the gateway. The solution to this is to configure the GLR nodes as end nodes, and a nearby OHT node as a relay node. OHTs that are not in the vicinity of any GLR can be conjured simply as an end node. The resulting network topology is a tree, and is shown in figure 1, with the end nodes corresponding to the ground level reservoirs shown as stars, the overhead tanks as red circles and the gateway as an arrow. The OHTs are numbered 1 through 5 and connect directly to the gateway. Similarly, each GLR communicates with the closest OHT in its vicinity. The gateway is mounted on a tower in the central administration building of the campus.

For this topology the measured signal quality in terms of the received signal strength (RSSI) and the packet error rate (PER) performance of the various links for different transmit power settings are shown in the Tables I & II. In these tables, the link number is the link coming out of the node with the same node number from figure 1, for the end nodes. For the relay nodes in the figure, the link corresponds to the link information from the relay node to the gateway.

TABLE I. RSSI AND PER PERFORMANCE OF RELAY TO GATEWAY LINKS FOR DIFFERENT TRANSMITTER POWER SETTINGS

Link No.	Distance (m)	14 dBm		10 dBm		5 dBm	
		RSSI	PER	RSSI	PER	RSSI	PER
1	200	-61.1	0	-64.7	0	-69.7	0
2	450	-68.1	0	-71.5	0.1	-77.5	2.7
3	570	-73.1	0	-76.4	0.2	-82.2	5.9
4	800	-83.5	0	-86.8	8.1	-89.6	88.1
5	1000	-80.2	0.3	-82.9	0.5	-86.6	10.3

TABLE II. RSSI AND PER PERFORMANCE OF END NODE TO RELAY LINKS FOR DIFFERENT TRANSMITTER POWER SETTINGS

Link No.	Distance (m)	14 dBm		10 dBm		5 dBm	
		RSSI	PER	RSSI	PER	RSSI	PER
2.1	80	-63	0	-66	0	-70.9	1.9
2.2	125	-103.9	4.9	-105.1	32.6	-107.1	97
3.1	30	-55	0	-58.7	0	-65.4	0
4.1	200	-95.1	0	-96.9	0	-101.8	0
4.2	225	-78.1	1.7	-81.1	14	-84.2	64.1
5.1	25	-49.5	0	-52.8	0	-56.8	0

TABLE III. POWER BUDGET

Module	Operating mode	Voltage	Current	Duration	Energy
Sensor	Active	5 V	300 mA	0.1 s	150 mJ
	Standby	0 V	0 A	59.9 s	0 J
Radio	Transmission	3.3 V	46 mA	24 ms	3.64 mJ
	Reception	3.3 V	19 mA	48 ms	3.01 mJ
	Reception standby	3.3 V	0.5 mA	10 ms	16.5 uJ
	Sleep	3.3 V	0.12 uA	59.918 s	23.7 uJ
Micro-controller	Active	3.3 V	24 mA	20 s	1.584 J
	Sleep	3.3 V	1 uA	40 s	132 mJ
Total					**1.873 J**

The links in Table II refer to the connection between each GLR and its corresponding OHT. For each link, in both these tables, the column corresponding to the shaded cells indicates the optimized power transmit power level chosen for the deployment that minimizes the power consumption. For cases with non-zero packet error rate, the higher level communication protocol, with retries, ensures that packets are eventually communicated.

V. Power System

Since the sensor nodes are deployed in high tanks, they need to be maintenance free as much as possible. Hence we have designed them to be powered by solar panels. The specifications of the battery and solar panel have been arrived at after taking into account the worst-case insolation during monsoon periods when there is significant cloud cover. The power supply is designed to supply 3.3V to the MSP432 microcontroller and the communication chip, and supply two programmable voltages, which are set to 5V and 12V for the sensor board, with power gating. NiMH batteries source the power, and a solar panel of rating 12W/12V is used to charge the batteries in two stages (buck converter followed by linear regulator) for efficient charging. The quiescent current of the power supply board is minimized to 3mA. The system takes a reading once every minute and transmits the same. Considering four 2200mAh batteries with a utilisation factor of 60%, we get around 15k cycles of operation, which makes the system work for approximately 10 days. This, in conjunction with a solar panel, enables the system to achieve continuous operation without needing frequent battery changes. The power budget is shown in table III.

VI. Results

The overall system block diagram is shown in figure 7. The designed sensor is fabricated and found to have a range of 10m with an accuracy of ±1.5% of full scale. The methodology for testing this is as follows: the sensors are set up in a corridor and a large Aluminium rectangular board is used as the reflector. The environment of the setup is indoors with minimal disturbances in the medium.

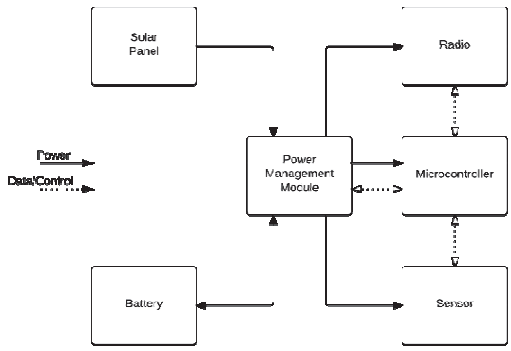

Fig. 7. System block diagram

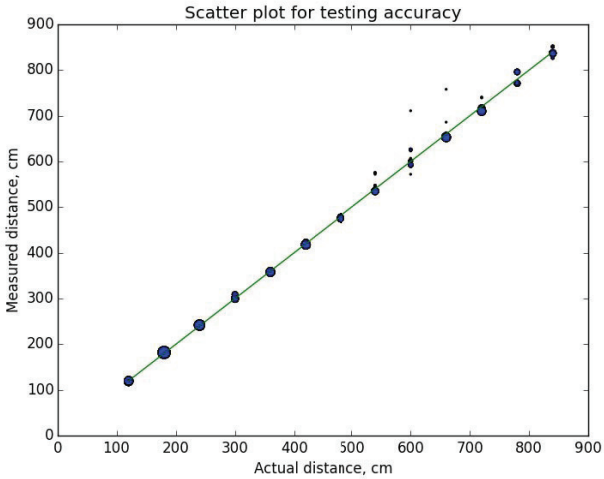

Fig. 8. Scatter plot of measured vs actual distance

Fifty readings are taken every 60 cm, and histograms are plotted at each distance. Finally, all the histograms are merged into a single scatter plot as shown in figure 8. The spots in this graph indicate the concentration of readings in an area. Clearly, accuracy is better at shorter distances. We determined that our sensor has an accuracy within ±1.5% of full scale, with improved accuracy at shorter distances. Further experiments at a swimming pool indicated the sensors performed with the same accuracy as that observed with the Aluminium board.

A picture of the installation of the sensor on a tank is shown in figure 9. The system was also installed in a Ground Level Reservoir (GLR) in the campus, with a relay placed on a nearby Overhead Tank (OHT) and the gateway setup a few hundred metres away. Data was collected every minute from the tank and was encapsulated into packets and transmitted to the relay, which then forwards it to the gateway. The gateway unpacks the received packet and uploads the level data online to a Google App Engine application. Figure 10 shows the collected data for half a day.

Fig. 9. Installation on a tank. The sensor transducer block is attached to the rim and freely hangs to ensure a vertical direction.

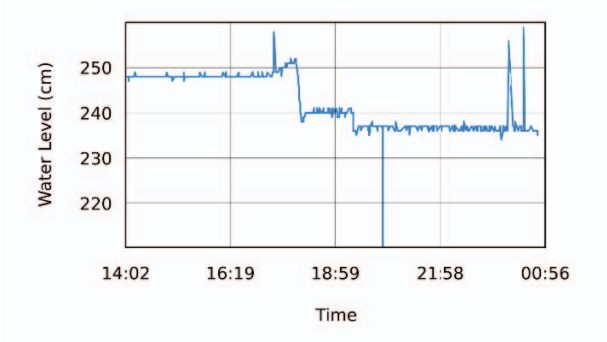

Fig. 10. Level data collected from a tank

A few glitches in the data can be seen that can be smoothed after acquisition. The variance in the readings is within 2 cm.

VII. Conclusions

We have described an IoT system consisting of custom sensors interconnected via a sub-GHz based wireless network. The sensor sub-system uses ultrasonic ranging to determine water levels in large tanks in the distribution system. Optimised circuitry and algorithm allowed achieving a range of up to 10 m with an accuracy within $\pm 1.5\%$ of full scale, using low cost transducers. Initial deployment results are encouraging and as a next step, we will instrument all the tanks. A further addition is to include control valves so that we can create a smart distribution system which distributes just enough water to each tank to satisfy the local demands.

Acknowledgment

We thank Mr. Alok Rawat for the design of the enclosure. We thank Mr. Sheetal Kumar and Ms. Anjana of Dept. of Civil Engineering, Indian Institute of Science, for discussions. We thank the Robert Bosch Centre for Cyber Physical Systems at Indian Institute of Science, Bangalore, for funding the project.

References

[1] UNDP. Human Development Report, Beyond Scarcity: Power, Poverty and the Global Water Crisis. United Nations Development Programme, 2006.

[2] UNDP. Human Development Report, Sustaining Human Progress: Reducing Vulnerability and Building Resilience. United Nations Development Programme, 2014.

[3] Food and Agriculture Organization of the United Nations. Coping with Water Scarcity: Challenge of the 21st Century. UNFAO, 2007.

[4] Amy Le. Liquid-Level Monitoring Using a Pressure Sensor. Texas Instruments, 2011

[5] Cytron Technologies. HC-SR04 Ultrasonic Sensor - Product User Manual, 2013.

[6] Vignesh Kudva, et al. Towards a real-time campus-scale water balance monitoring system. In VLSI Design, 2014.

[7] Ivan Stoiano. Lama Nachman. Sam Madden. Pipenet: A wireless sensor network for pipeline monitoring. In IEEE International Symposium on Information Processing in Sensor Networks, Cambridge, Massachusetts, 2007.

[8] Ch. Papageorgiou and Th. Laopoulos. Modification of resonance characteristics of ultrasonic transducers by the driving circuit. In Proc. of XVII IMEKO World Conference, Dubrovnik 2003.

[9] Gary Petersen. L-matching the output of a RITEC gated amplifier to an arbitrary load. 2006.

[10] Raymond S. Frenkel. Coded pulse transmission and correlation for robust ultrasound ranging from a long-cane platform. Master's thesis, University of Massachusetts - Amherst, 2008.

[11] Nihesh Rathod. et al. Performance analysis of wireless devices for a campus-wide IoT network. In Wireless Networks: Measurements and Experimentation Workshop, held in conjunction with WiOpt 2015 Conference, Mumbai 2015.